Supplemental Material: Acoustic Topological Transport and Refraction in a Kekulé Lattice

Boyang Xie[1], Hui Liu[1], Hua Cheng[1,3],[*] Zhengyou Liu[2], Shuqi Chen[1,3,4],[†] and Jianguo Tian[1,3]

[1]*The Key Laboratory of Weak Light Nonlinear Photonics, Ministry of Education,*

School of Physics and TADA Institude of Applied Physics,

Nankai University, Tianjin 300071, China

[2]*School of Physics and Technology and Institute for Advanced Studies,*

Wuhan University, Wuhan 430072, China

[3]*Renewable Energy Conversion and Storage Center,*

Nankai University, Tianjin 300071, China and

[4]*The collaborative Innovation Center of Extreme Optics,*

Shanxi University, Taiyuan, Shanxi 030006, China

(Dated: February 18, 2019)

1. EDGE STATES AROUND VALLEYS

The valley transport arise between the first and second band with zigzag domain wall $Z'_{\mathrm{I,II}}$ and $Z'_{\mathrm{II,I}}$ [Fig. 7(e, f)]. When we fix $r_{\mathrm{B}} = 0.260a$ and gradually increase r_{A}, the bulk degeneracy at K is lifted and the edge states appear as simulation edge bands shown in Fig. S1.

2. DECAY

The decay coefficient along the domain wall is measured by fitting the exponential function [Fig. S2(a)]. The decay along the domain wall is caused by intrinsic loss of airborne sound and imperfectness of sample. Here we only show the data that the fitting coefficient of determination is above 95%. A key feature of the topological edge state is the exponential decay of the field amplitude away from the domain wall. To confirm this, we also scan the pressure field along a straight line vertical to the domain wall [Fig. S6(b). Our configuration of interlaced small and big rods shows larger decay rate vertical to the domain wall than the configuration proposed by He *et. al*, which means the energy of sound wave is more concentrated to the domain wall.

3. SIMULATED OUT-COUPLING ANGLE

Figure S3 plots the simulated out-coupling field patterns for $Z_{\mathrm{I,II}}$ and $Z_{\mathrm{II,I}}$ domain wall and armchair terminations. The refraction angle for $Z_{\mathrm{I,II}}$ domain wall is slightly smaller than $Z_{\mathrm{II,I}}$. The refraction angle become smaller for higher frequency due to the phase-matching demonstrated in Fig. 4a. The out-coupling beams exhibits a high-directivity performance.

4. REFLECTION AT TERMINATION OF THE SONIC CRYSTAL

Figure S4 shows the simulated reflection obtained by transfer function method at termination vertical to $Z_{\mathrm{I,II}}$, $Z_{\mathrm{II,I}}$ and armchair (AC) interfaces. The non-negligible reflection at termination may cause inevitable excitation of time-reversal counterpart of pseudospin and Fabry-Perot resonance in the waveguide.

5. EDGE STATES AT CROSSING CHANNELS

Figure S5 shows the partition of edge states at crossing zigzag or armchair interfaces. The angle between the horizontal and tilted interfaces is 60°. The transfer into channel D is dominant due to greater spatial overlap of the edge modes between L and D channels. The reflected wave from the termination of D may transfer into R channel when the direct coupling of edge mode between L and R channels is forbidden.

6. TOPOLOGICAL PHASE WITH VARYING RADIUS

In Fig. S6, we show the bandgap ratio of the edge states to the bulk states with varying r_A, r'_A and fixed $r_B = 0.260a$, $r'_B = 0.173a$, where the topological edge states appear in the gapless region (blue color scale) indicating that the two domains beside the interface are topological different. The M1 zone in the up-left corner is mainly caused by the breaking of inversion symmetry, while the M2 zone in the down-right corner is caused by topological transition tuned by the filling ratio.

7. VORTEX OF EDGE STATES AROUND THE DOMAIN WALL

The phase distributions are scanned around the rods near the domain wall as shown in Fig. S7. The experimentally measured phase distributions (points with error bar) agree well with those extracted from the simulation (lines). The vortexes around the big rods and small rods carry opposite angular momenta. Also, the vortexes in domain II carry opposite angular momenta compared with vortexes in domain I. The phase distributions indicate the two domains have different pseudospins.

8. METHODS

Experiments. The experiments are performed in a 2D waveguide system with the height of 2 cm. In experiments, several hundreds of resin rods fabricated by 3D printing are arranged into desired sample configurations. The rods are closely sandwiched between two acoustically rigid parallel plates. The sound signal is launched from a loudspeaker in the sonic crystal and scanned with a movable microphone (of diameter 0.64 cm, B&K Type

4961), while another identical microphone is fixed which serves as the phase reference. The acoustic signal is analyzed by a multi-analyzer system (B&K Type 3560B), with which both the amplitude and phase of the wave are extracted. The whole waveguide is surrounded by the acoustical absorbent material, intending to reduce the reflection from the impedance mismatch between the sample and free space.

Simulations. All full-wave simulations are conducted using the pressure acoustic module of a commercial software based on the finite element method (COMSOL Multiphysics), where the resin rods used in real experiments are modeled as acoustically rigid, considering the great impedance mismatch with respect to air (density $\rho = 1.2$ kg/m^3 and speed of sound $c = 343$ m/s). The whole structure is modeled as a 2D system, as the propagating mode is uniform in the z-direction for the frequency under consideration.
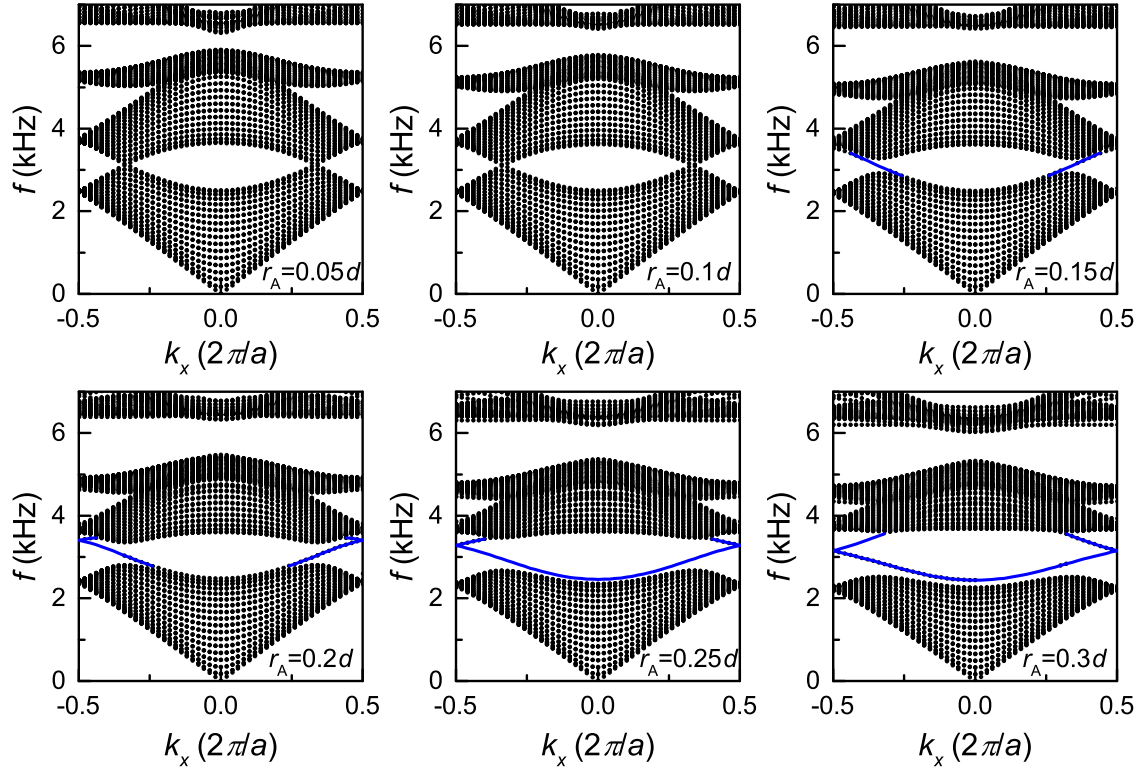
----

* hcheng@nankai.edu.cn

† schen@nankai.edu.cn

FIG. S1. Simulated band dispersions for the $Z'_{\mathrm{I,II}}$ with fixed $r_{\mathrm{B}} = 0.260a$. The bulk bands are in black dots and the edge bands are in blue lines.
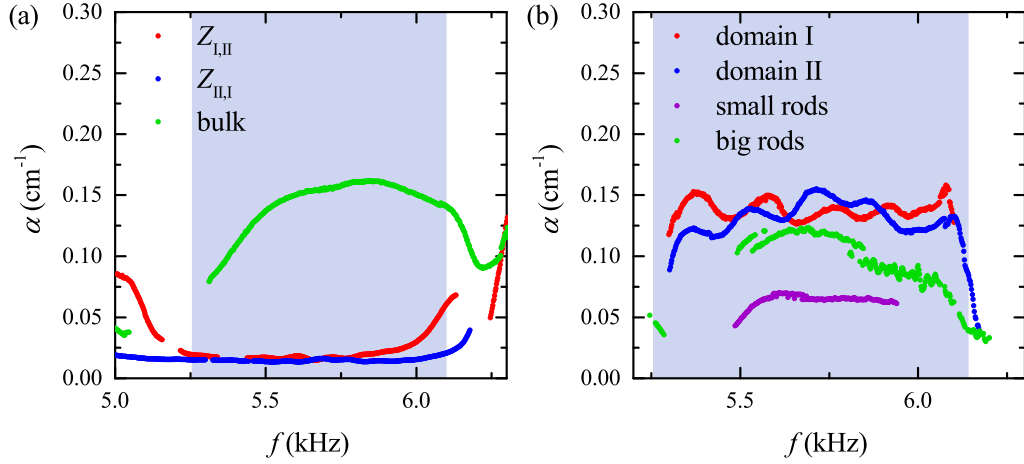
FIG. S2. Experimental decay coefficient (a) along or (b) vertical to the propagating direction. The shaded regions represent the theoretical bulk gap. Exponential function fitting have been employed to evaluate the decay coefficient. We only show the data that the fitting coefficient of determination is above 95%.
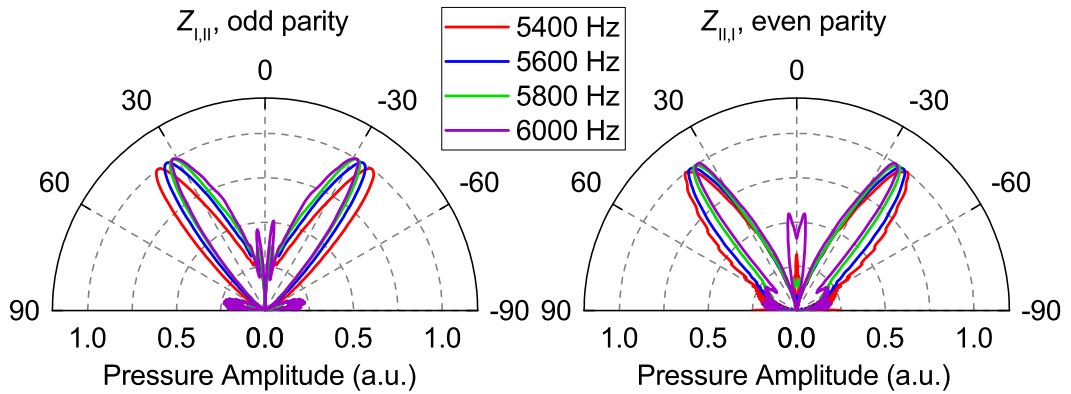

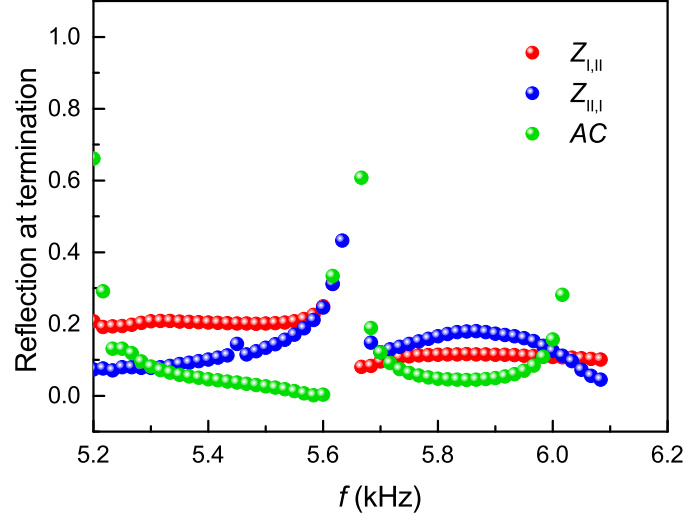FIG. S3. Polar plot of the simulated radiation patterns for out-coupling field pattern.

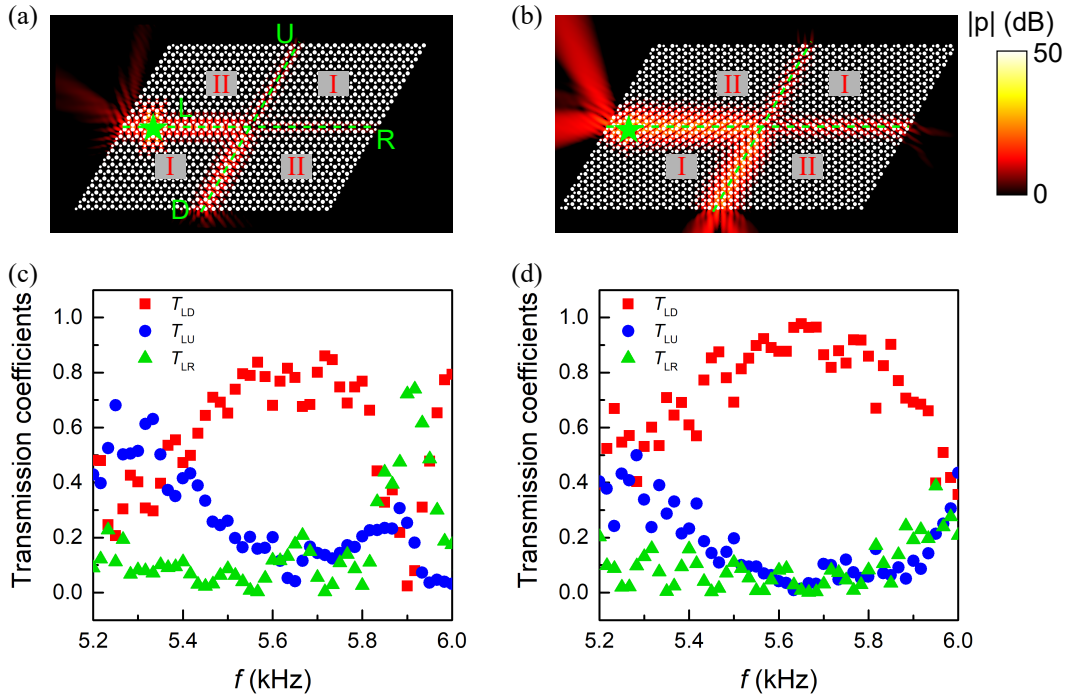FIG. S4. Reflection at termination of the sonic crystal.

FIG. S5. (a,b) Simulated pressure amplitude for crossing (a) zigzag and (b) armchair interfaces at frequency of 5.6 kHz. The domains I and II form four interfaces denoted as green dashed lines and labeled as L (left), R (right), U (up) and D (down). (c,d) The transmission spectrum with (c) zigzag or (d) armchair interfaces. The position of the source is indicated by a green star near the left end of the interface.
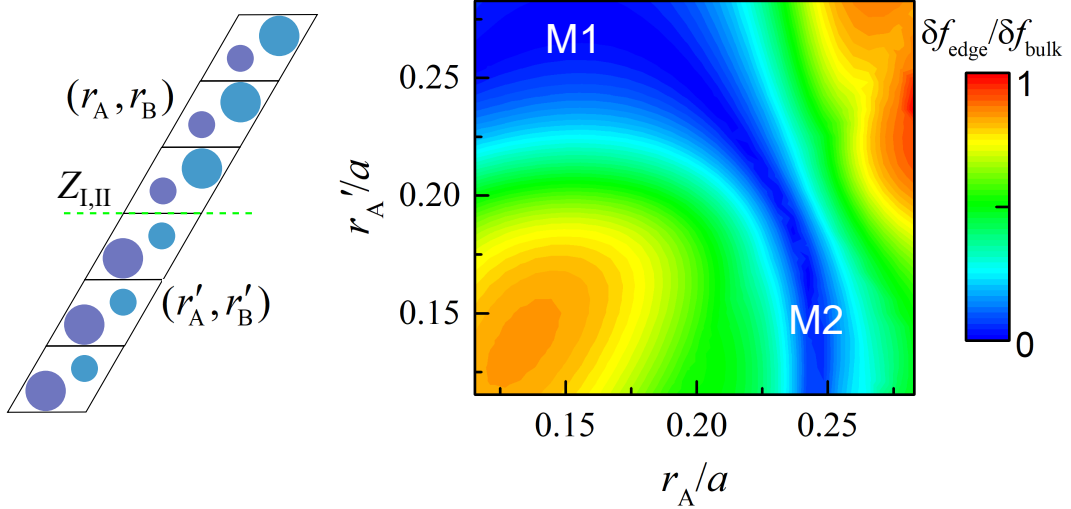
FIG. S6. (f) The bandgap ratio of the edge states to the bulk states with varying r_A, r'_A and fixed $r_B = 0.260a$, $r'_B = 0.173a$, where the topological edge states appear in the gapless region (blue color scale). The M1 zone in the up-left corner is mainly caused by the breaking of inversion symmetry, while the M2 zone in the down-right corner is caused by topological transition tuned by the filling ratio.
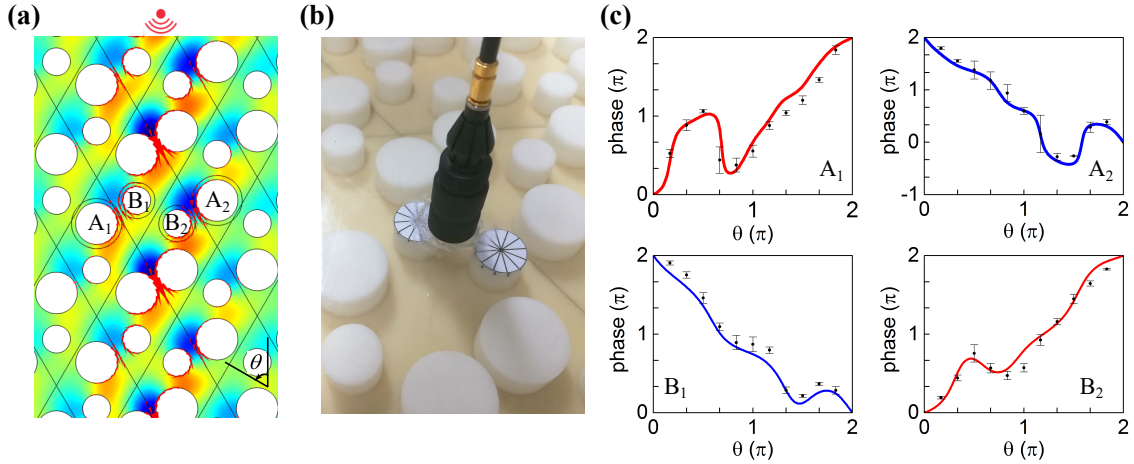

FIG. S7. (a) Simulated pressure field distribution of edge states along armchair domain wall. (b) Schematic of the experimental setup. (c) Phase distributions simulated (lines) and measured (points with error bar) anticlockwise along a circular trajectory around the A and B rods in two different domains. The red and blue line indicate quantized angular momenta 1 and -1, respectively.